Ultrasound in Med. & Biol., Vol. 31, No. 5, pp. 599–605, 2005

0301-5629/05/$–see front matter

ELSEVIER

doi:10.1016/j.ultrasmedbio.2005.01.009

● *Original Contribution*

LIVER STEATOSIS CLASSIFICATION USING HIGH-FREQUENCY ULTRASOUND

WEN-CHUN YEH,* YUNG-MING JENG,† CHENG-HAN LI,* PO-HUANG LEE,‡ and PAI-CHI LI*
*Department of Electrical Engineering, National Taiwan University, Taipei, Taiwan; and †Department of Pathology and ‡Department of Surgery, National Taiwan University Hospital, Taipei, Taiwan

(*Received* 20 *September* 2004; *revised* 12 *January* 2005; *in final form* 27 *January* 2005)

Abstract—High-frequency B-mode images of 19 fresh human liver samples were obtained to evaluate their usefulness in determining the steatosis grade. The images were acquired by a mechanically controlled single-crystal probe at 25 MHz. Image features derived from gray-level concurrence and nonseparable wavelet transform were extracted to classify steatosis grade using a classifier known as the support vector machine. A subsequent histologic examination of each liver sample graded the steatosis from 0 to 3. The four grades were then combined into two, three and four classes. The classification results were correlated with histology. The best classification accuracies of the two, three and four classes were 90.5%, 85.8% and 82.6%, respectively, which were markedly better than those at 7 MHz. These results indicate that liver steatosis can be more accurately characterized using high-frequency B-mode ultrasound. Limitations and their potential solutions of applying high-frequency ultrasound to liver imaging are also discussed. (E-mail: paichi@cc.ee.ntu.edu.tw) © **2005 World Federation for Ultrasound in Medicine & Biology.**

Key Words: **High-frequency ultrasound, Tissue characterization, Gray-level concurrence, Nonseparable wavelet transform, Support vector machine, Liver pathology, Steatosis.**

INTRODUCTION

Hepatic steatosis (the accumulation of fat within liver cells) is a common histologic finding in liver biopsies (Teli et al. 1995). Steatosis can be classified as microvesicular or macrovesicular, depending on the morphology and size of lipid droplets. Microvesicular steatosis occurs in a variety of inherited and acquired disorders that share a final common pathway of defective β-oxidation of free fatty acids, such as acute fatty liver of pregnancy and Reye's syndrome. Macrovesicular steatosis is frequently seen in patients with obesity, alcoholic liver disease, insulin resistance diabetes, a wide variety of drug-induced and inherited metabolic disorders and hepatitis C (Angulo 2002; Brunt 2001). Macrovesicular steatosis in nonalcoholic patients is widely believed to be a benign condition with little or no risk of disease progression. However, marked macrovesicular steatosis may result in necroinflammation, fibrosis and even cirrhosis (Brunt 2001; Teli et al. 1995). This kind of liver injury in nonalcoholic patients, known as nonalcoholic steatohepatitis (NASH) or nonalcoholic fatty liver disease, has been widely investigated (Angulo 2002). Brunt et al. (1999) proposed a grading and staging system for histologic examinations of NASH, which included the steatosis grade as determined by the percentage of affected hepatocytes. They found that the mean value of serum liver enzymes increased with the grade of NASH. Clinically, patients with mildly elevated levels of serum liver enzymes are not always subjected to invasive studies (*e.g.,* liver biopsy) that can help determine the cause of hepatitis. B-mode ultrasound is usually recommended as a first step and it has been used to classify liver tissue. Yang et al. (1988) developed a scoring system to evaluate the severity of liver steatosis based on several image characteristics such as echogenicity, attenuation and masking of the portal vein or gall bladder. Steatosis can also be classified on the basis of image features. Mojsilovic et al. (1998) proposed a nonseparable wavelet transform (NSW) method to extract the B-mode image features for the classification of healthy liver, cirrhosis and steatosis. However, the spatial resolution of B-mode ultrasound at lower frequencies ($\leq$10 MHz) is generally inadequate for revealing morphologic changes of steatosis and for estimating the percentage of hepatocytes affected.

High-frequency ultrasound ($\geq$20 MHz) has been used to investigate skin structures (Raju et al. 2003), eyes

Address correspondence to: Pai-Chi Li, Department of Electrical Engineering, National Taiwan University, No. 1, Sec. 4, Roosevelt Road, Taipei 106, Taiwan. E-mail: paichi@cc.ee.ntu.edu.tw

(Nouby-Mahmoud et al. 1993), blood vessels (Nissen and Yock 2001), myocardium (Dent et al. 2000) and small-animal embryos (Foster et al. 2002; Li et al. 2004). Nevertheless, high-frequency ultrasound has not been widely applied to the characterization of liver tissue, primarily due to its limited penetration. For example, Fox and Pruehsner (1997) used 8- to 20-MHz ultrasound to analyze liver and cardiac tissues *in vitro* based on the signal spectrum and Yoshihara et al. (1998) used 30- to 70-MHz ultrasound on hen livers and found that the attenuation patterns of the ultrasound differed between normal and steatosis livers. Petersen (2003) used intravascular ultrasound in inferior vena cava to guide the puncturing for an intrahepatic portacaval shunt. Good resolution of the hepatic structures and the image guide were helpful in completing the procedure with minimal complications. Although the center frequencies of the catheter transducers in his system were less than 10 MHz, other intravascular ultrasound systems operating at higher frequencies can also be applied (Nissen and Yock 2001). The intravascular approach provides a potential solution for the application of high-frequency ultrasound to the human liver. Inserting the imaging catheter into the hepatic veins from the inferior vena cava allows the ultrasound to penetrate deeper into the liver, because the vessel walls are thinner in the branches of hepatic veins (Wachsberg et al. 1997). In this study, we evaluated the feasibility of tissue characterization of the human liver using 25-MHz B-mode ultrasound *in vitro*. The initial experiments revealed promising preliminary results. Some qualitative similarities can be found in comparison of the histologic images of steatosis livers with the 25-MHz ultrasound images. Figure 1a shows that the steatosis-affected hepatocytes (grade 1) were located mainly in the central area of the acinus and that the clusters of affected hepatocytes appeared to be oval (indicated by the arrow). The 25-MHz ultrasound image shows a similar pattern to the clusters of affected hepatocytes shown in Fig. 1a (indicated by the arrow in Fig. 1b). Figure 1c shows that the steatosis-affected hepatocytes in another liver (grade 1) were located mainly in the periportal area (indicated by the arrow). Again, the 25-MHz B-mode image in Fig. 1d presents a similar pattern (indicated by the arrow). Also, comparison of the 25-MHz ultrasound images of a mild steatosis liver with those of a severe-steatosis liver revealed that brightened lesions (representing the steatosis areas) occupy larger areas in the latter. Thus, 25-MHz B-mode ultrasound seemed to have the ability to reveal detailed morphologic changes of steatosis. The results of this feasibility study could form the foundation of the use of intravascular high-frequency ultrasound in liver disease classification.

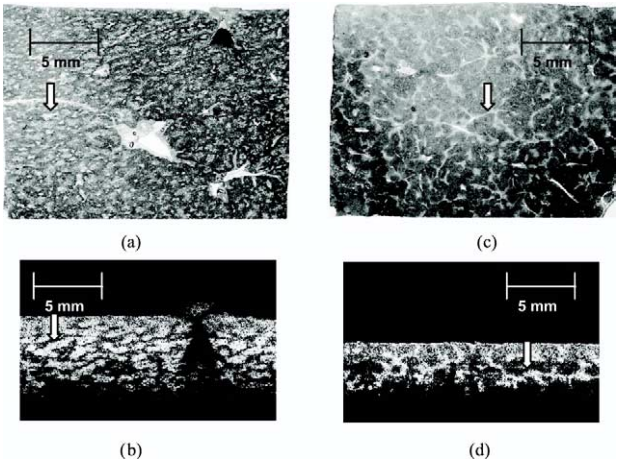

Fig. 1. (a) and (c) Low-magnification images of two steatosis livers with Masson's trichrome stain; image size is 21.0 × 16.0 mm. (b) and (d) The corresponding 25-MHz ultrasound images; image size is 18.6 × 11.8 mm. The steatosis patterns (arrows in (b) and (d)) in the 25-MHz ultrasound images are very similar to those in the low-magnification images (arrows in (a) and (c)).

MATERIALS AND METHODS

Image feature extraction and classification

The increase in echogenicity of liver relative to that of the kidneys associated with steatosis has been utilized in clinical diagnoses (Joseph et al. 1991). However, computer-aided diagnosis requires more image features. The present study adopted the gray-level concurrence (GLC) (Wu et al. 1992) and NSW (Mojsilovic et al. 1998) methods to classify steatosis grades using the support vector machine (SVM), a classification technique proposed by Cortes and Vapnik (1995).

In the GLC method, a spatial gray-level dependence matrix (*i.e.*, the concurrence matrix) is first calculated (Haralick 1973). The matrix, $Co(i,j;d,\theta)$, represents the probability that the first pixel has a gray level of i and the second pixel has a gray level of j under the condition that the distance between the two pixels is d in the direction θ (Wu et al. 1992). Figures 2a and 2b show the concurrence matrices ($d = 6$, $\theta = 0°$) of 25-MHz ultrasound images of a steatosis liver and a nonsteatosis liver, respectively. Generally, the probability pattern of the concurrence matrix of a steatosis liver has a wider distribution than that of a nonsteatosis liver. Image features such as the angular second moment, contrast, correlation, entropy and sum entropy can be derived from the concurrence matrix (Wu et al. 1992; Yeh et al. 2003).

In addition to GLC, NSW was also applied to extract the image features, using the quincunx wavelet transform (Mojsilovic et al. 1998; Yeh et al. 2003). In this case, the original image was filtered by a 2-D diamond-shaped high-pass filter and a low-pass filter of the same shape before it was downsampled to a new image

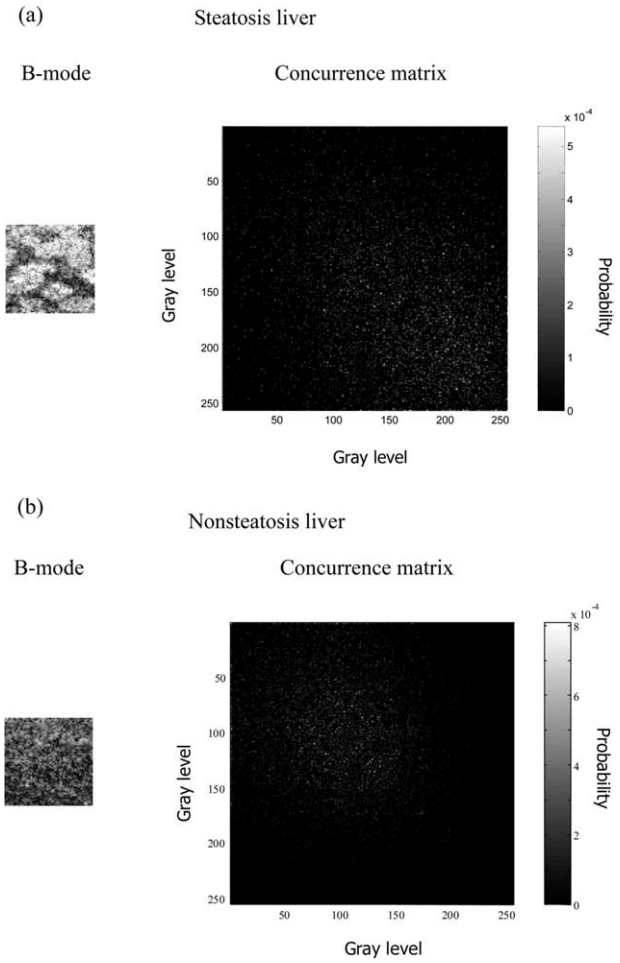

Fig. 2. B-mode subimages of 25-MHz ultrasound with their corresponding concurrence matrices in (a) a steatosis liver (grade 1) and (b) a nonsteatosis liver.

with half the original area. Filtering and downsampling were performed four times, thus producing high-pass-filtered subimages H1–H4 and low-pass-filtered subimages L1–L4. The variances of images H1–H4 and L4 were taken as the image features (Mojsilovic et al. 1998; Yeh et al. 2003). Figure 3 compares the NSW output images of a steatosis liver (Fig. 3a) with those of a nonsteatosis liver (Fig. 3b) (25-MHz ultrasound). In this particular case, the variances of the output images (H1–H4 and L4) of the steatosis liver (1037.1, 568.3, 376.4, 416.4 and 1529.5, respectively) exceed those of the nonsteatosis liver (964.1, 465.5, 243.8, 177.2 and 428.4, respectively).

The features extracted by the above two methods were used for classification. This study used the SVM as a classifier. The SVM maps features of the training examples to a higher dimensional space and finds a hyperplane to separate the two classes with the decision boundary set by the support vectors (Burges 1998; Chan et al. 2002). A multiclass SVM classifier developed by Junshui Ma (NIS-2, Los Alamos National Laboratories, USA) and Yi Zhao (Electrical Engineering Department, Ohio State University, USA) was used in this study (see http://www.csie.ntu.edu.tw/~cjlin/libsvm).

Image acquisition and processing

Nineteen fresh human liver samples obtained from surgical specimens were studied. Among them, 13 samples had hepatitis B virus (HBV) infection, three samples had hepatitis C virus (HCV) infection and the others had no evidence of HBV or HCV infection. These specimens were cut into bar shapes (3 to 5 cm wide, 2 to 3 cm thick and 5 to 6 cm long) and immersed in normal saline. After scanning by 25- and 7-MHz ultrasound, the specimens were graded for steatosis histologically.

High-frequency ultrasound (25 MHz)

A lithium-niobate single-crystal focused transducer (NIH Resource Center for Medical Ultrasonic Transducer Technology, Penn State University, USA) was used. The center frequency of the transducer was 44 MHz (−6 dB bandwidth: 34 to 59 MHz). The transducer had a diameter of 6 mm and was geometrically focused at 12 mm. The distance from the probe to the surface of the liver samples was initially set to 10 mm. An arbitrary-function generator (DAC200, Signatec, Corona, CA, USA) was used to generate the desired transmit waveform, which was sent to a power amplifier (25A250A, Amplifier Research, Souderton, PA, USA) to drive the lithium-niobate focused transducer. A three-axis motor system with the precision of 1 μm (SMAC, Taipei, Taiwan) was used to control the relative position between the target and the transducer. To extend the depth of focus of the fixed-focus transducer, two images

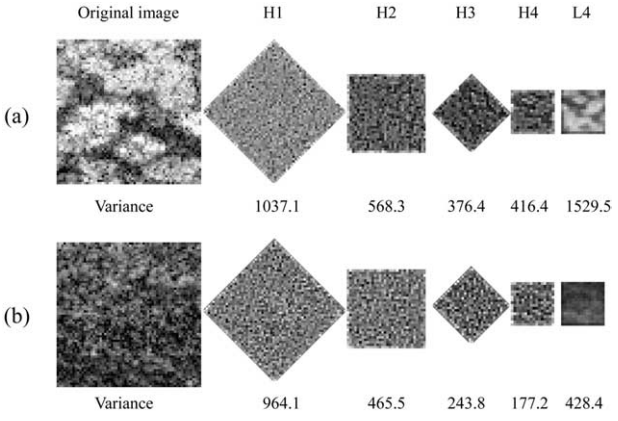

Fig. 3. Nonseparable wavelet transform of (a) a steatosis liver (grade 1) and (b) a nonsteatosis liver. H1–H4: images after high-pass filtering and downsampling. L4: image after final low-pass filtering and downsampling.

were acquired and combined (also known as a depth scan). The two images corresponded to two transducer positions separated by 2 mm in the axial direction (Passmann and Ermert, 1996). The scan-line data acquired at each position were detected by an ultrasonic receiver (5900, Panametrics, Waltham, MA, USA). Finally, the signal was sampled with an analog-to-digital converter at 200 Msamples/s with an 8-bit resolution (PDA500, Signatec) and recorded on the hard disk of a personal computer.

For 25-MHz imaging, three cycles of a sine-wave pulse with a center frequency of 25 MHz were transmitted. Note that 25 MHz was used instead of the center frequency of transducer, because 44 MHz did not have adequate penetration depth required by this study. The spacing between two adjacent scan lines was 20 μm. The scanning distance was 20 mm and the scanning time was 0.2 s for each frame. The signal-to-noise ratio at the focal point was around 30 dB. All images in this paper are displayed with a 36-dB dynamic range.

Conventional ultrasound (7 MHz)

After the 25-MHz data were acquired, the same specimen was scanned using a 7-MHz linear-array transducer (10L/LOGIQ 500, GE, Chalfont St. Giles, UK) in a water tank. Three-dimensional data were acquired whilst using a stepper motor to move the probe. The images were then acquired using a frame grabber (UPG401B, UPMOST, Taipei, Taiwan) with 256 gray levels and 320 × 240 pixels per image.

Image processing

A subimage of 64 × 64 pixels (11.0 × 11.0 mm and 2.8 × 2.8 mm, equivalent to 51.3 × 51.3 λ and 46.7 × 46.7 λ for 7- and 25-MHz, respectively, where λ is the ultrasound wavelength) was selected from each image. Areas of blood vessels and image artifacts, such as shadowing, were avoided. Ten subimages at each frequency were selected for each specimen; the cross-correlation coefficients among the images were all below 0.5. Gray-scale mapping was not adjusted, because the gain and the dynamic range were fixed during image acquisition. Image features were extracted using the GLC and NSW methods from these subimages.

After ultrasound scanning, the specimens were fixed in formalin and embedded in paraffin. Several sections were cut from each specimen at a thickness of 5 μm and stained with Masson's trichrome stain for histologic examination. Slices of all specimens were photographed with a digital camera (S85 Sony, Tokyo, Japan) under low magnification (3×). The steatosis grade was classified by an experienced pathologist according the following criteria (Brunt et al. 1999): 0, no fatty change; 1, less than 33% of hepatocytes affected; 2, 33 to 66% of hepatocytes affected; and 3, more than 66% of hepatocytes affected. A semiautomatic method to calculate the percentage of affected hepatocytes was also adopted to verify the results of steatosis grading. The liver slices were also photographed at high magnification (30×) with a digital camera (Coolpix 4500, Nikon, Tokyo, Japan) mounted on a microscope (XTL 300A, Teng-Bo, Taipei, Taiwan). The digitized images were then sent to a personal computer and processed using commercial image processing software (Photoshop version 4.0.1 TC, Adobe, San Jose, CA, USA). The hepatocytes affected by steatosis (black arrow in Fig. 4a) are shown in white in Fig. 4b; unaffected hepatocytes are gray and the other tissues, such as fibrosis regions (white arrow in Fig. 4a), are black. The percentage of steatosis can be calculated as the number of affected hepatocytes (number of white pixels in Fig. 4b) divided by the total number of hepatocytes (number of white and gray pixels) and the steatosis grade can be determined. The four grades of steatosis were then combined into two, three and four classes according to the following criteria: two classes (grade 0 and grades 1 to 3; representing nonsteatosis and steatosis), three classes (grade 0, grade 1, and grades 2 and 3; representing nonsteatosis, mild steatosis and obvious steatosis) and four classes (all four grades). The classification accuracy was tested using the SVM by the leave-one-out method (Ney et al. 1995; Weiss 1991). After testing, the classification results were recorded. The process was repeated until all images had been tested. The accuracy was then determined as

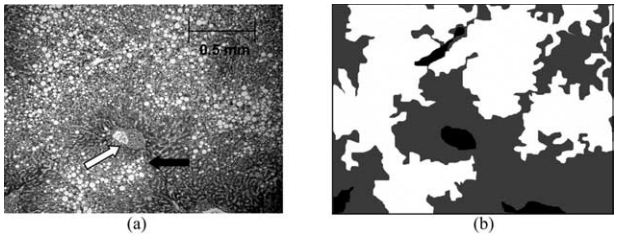

Fig. 4. (a) A high-magnification image of a steatosis liver (grade 2) with Masson's trichrome stain; image size is 2.1 ×1.6 mm. (b) The steatosis-affected hepatocytes (black arrow in (a)) are shown in white, unaffected hepatocytes are gray and the other tissues (white arrow in (a)) are black.

$$\text{Accuracy} = \frac{CI}{N}, \tag{1}$$

where CI is the number of correct incidences in a particular class and N is the total number of samples in that class. Various combinations of input features (angles and distances of GLC; filter pairs of NSW) and SVM parameters (penalty term and kernel-function parameters) were tested to determine the best performance achievable (Yeh et al. 2003).

Table 1. Mean percentage of steatosis and grading of ten specimens of steatosis livers by the semiautomatic method and by the pathologist

Specimen no.	1	2	3	4	5	6	7	8	9	10
Mean percentage	9.5	49.2	12.6	14.5	34.4	75.9	4.3	17.8	2.2	18.0
Semiautomatic	1	2	1	1	2	3	1	1	1	1
Pathologist	1	2	1	1	2	3	1	1	1	1

RESULTS

The numbers of specimens in each steatosis grade are as the following: nine in grade 0, seven in grade 1, two in grade 2 and one in grade 3. Table 1 lists the mean steatosis percentages (calculated from five different images of each specimen) and the grading results of the 10 steatosis specimens using the semiautomatic method and also by the pathologist. It was verified that the grading results were the same by both methods. All the classification results herein were estimated with a Gaussian radial-basis function kernel, since this outperformed the polynomial kernel. Table 2 presents the classification accuracy obtained using the GLC features and the NSW features. It shows that the accuracy of the NSW is better than that of the GLC. Combining features slightly improves the performance. The combination of all features of the GLC ($d = 6$, $\theta = 0°$) and all features of the filter pair B of NSW (as defined in Yeh et al. 2003) yielded the best results among all the different combinations. For 25-MHz ultrasound images, the best classification accuracies of the two, three and four classes were 90.5%, 85.8% and 82.6%, respectively, as shown in Table 3, which were markedly better than those for conventional ultrasound at 7 MHz (best classification accuracies of 81.6%, 75.8% and 74.2%, respectively).

DISCUSSION AND SUMMARY

The 25-MHz images resulted in more accurate steatosis classification. The Figure 6 compares the images for 25- and 7-MHz ultrasound. The hepatocytes affected by steatosis in the high-magnification image (indicated by the arrow in Fig. 5a) appear as bright oval or strip-shaped structures in the low-magnification image (indicated by the arrow in Fig. 5b). Furthermore, the pattern of steatosis distribution in Fig. 5b is more clearly demonstrated in the 25-MHz ultrasound image (indicated by the arrow in Fig. 5c) than in the 7-MHz ultrasound image (indicated by the arrow in Fig. 5d). Because the spatial resolution is directly related to the frequency, the 25-MHz images resembled the low magnification optical images, while the 7-MHz images did not contain the details.

On histologic sections, fat in the liver appears as a globular intracytoplasmic clear space, since the fat is removed by routine tissue processing that leaves only the shape interface that the lipid body forms with the remaining aqueous cytoplasm (Edmonson and Peters 1985). Liver steatosis is usually graded using slices stained with hematoxylin and eosin (Brunt et al. 1999). With Masson's trichrome stain, the fatty droplets can still be recognized easily and the fibrosis tissue can also be demonstrated clearly (Fig. 4a).

The degree of liver fibrosis ranges from fibrous expansion in the portal area to cirrhosis (Edmonson and Peters 1985). Fibrosis and steatosis often coexist in the liver. Steatosis induces fibrosis and HBV hepatitis is also complicated with steatosis. Detections of fibrosis and steatosis grades are both needed in liver tissue characterization. In our 19 liver samples, 13 had HBV infection, three had HCV infection and the others had no evidence of HBV or HCV infection. All samples had fibrosis (7 cirrhosis, 12 noncirrhosis). Among the 10 steatosis cases, two had cirrhosis. Using GLC and NSW,

Table 2. The classification accuracy

Method	Accuracy (%)						
	GLC (d = 6)				NSW		
Group	1	2	3	4	A	B	C
2	83.7	81.6	82.1	81.6	90.5	88.4	87.9
3	74.7	74.2	76.3	73.7	84.7	77.9	82.1
4	70.0	70.5	74.7	71.1	82.6	75.8	79.5

GLC: gray-level concurrence; NSW: nonseparable wavelet transform; d: distance of pixels, 1: $\theta = 0°$, 2: $\theta = 45°$, 3: $\theta = 90°$ and 4: $\theta = 135°$ for the GLC; A, B, C: different filter pairs for the NSW as defined in Yeh et al. (2003).

Table 3. The classification accuracy with combined features

Number of classes	Accuracy in different steatosis grade (%)				
	3	2	1	0	Overall
2		90		91	90.5
3	66.7		81.4	95.6	85.8
4	20.0	65.0	82.9	93.3	82.6

we have compared the image features of a cirrhotic liver with those of a steatosis liver. Generally speaking, values of the GLC and the NSW image features lie in different ranges among a cirrhotic liver, a steatosis liver and a nonsteatosis/ noncirrhotic liver. Nonetheless, the classification accuracy decreased when we attempted to differentiate different steatosis grades from fibrosis grades. The decrease may be due to the inherent limitation of such a classification approach, but may also be partly due to the limited number of liver samples in each individual combination of steatosis and fibrosis grades.

High-frequency ultrasound provides better spatial resolution and reveals more details of steatosis than does conventional ultrasound (operating at lower frequencies), but its clinical applications are limited by intraabdominal organs being difficult to visualize, because high frequency sound waves cannot penetrate the abdominal wall. The intravascular approach may be a potential solution to this problem. In addition to the limited penetration, the small depth of focus of the single-crystal probe creates another limitation. For example, fibrosis patterns, especially cirrhosis, may not be adequately demonstrated using high-frequency ultrasound. The diameter of regenerative nodules (the key feature for the pathologic diagnosis of cirrhosis) is generally greater than 3 mm in patients with late-phase of hepatitis-B cirrhosis (Edmonson and Peters 1985). We have previously classified the fibrosis grade by SVM using 7-MHz ultrasound (Yeh et al. 2003) and the increased spatial resolution of 25-MHz may not improve the classification of fibrosis, due to the limited penetration and the small depth of focus. Nevertheless, the depth of focus can be increased by using a high-frequency array transducer with dynamic focusing (Buma et al. 2003).

Among the 10 steatosis cases investigated here, two cases with very mild steatosis in the central area of the acinus presented inhomogeneous brightened lesions in the 25-MHz ultrasound images (Fig. 6a). Figure 6b shows the magnified region of interest (white window in Fig. 6a), in which the intensity of the central parts (indicated by the triangle) is higher than that of the surrounding parts of the brightened lesions (indicated by the arrows). Correlating with the high-magnification im-

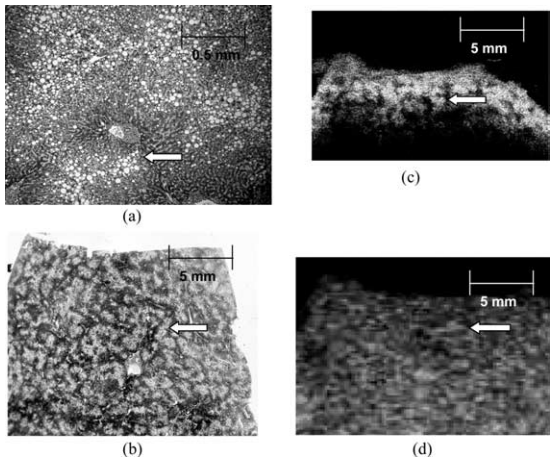

Fig. 5. (a) A high-magnification image of a steatosis liver (grade 2) with Masson's trichrome stain; image size is 2.1 × 1.6 mm. Hepatocytes affected by steatosis are indicated by the arrow. (b) A low-magnification image with Masson's trichrome stain; image size is 19.6 × 16.0 mm. Hepatocytes affected by steatosis are shown as light gray (arrow). (c) The corresponding 25-MHz ultrasound image; image size is 18.6 × 11.8 mm. The steatosis regions appear bright (arrow). (d) The corresponding 7-MHz ultrasound image; image size is 20.0 × 15.0 mm. The margins of steatosis areas are not clearly evident (arrow) at 7 MHz.

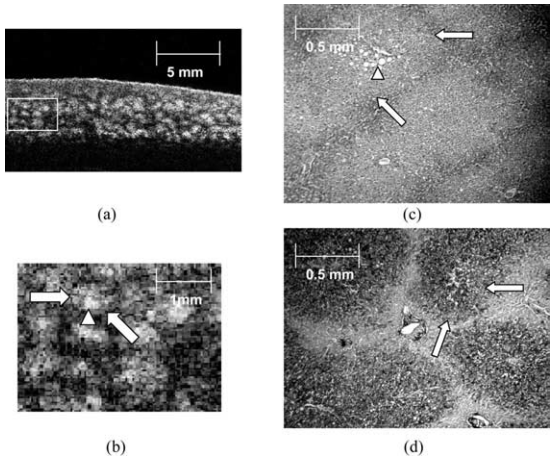

Fig. 6. (a) A 25-MHz ultrasound image of a steatosis liver (grade 1); image size is 18.6 × 11.8 mm. (b) Magnified B-mode image of the region-of-interest (white window in (a)); image size is 4.0 × 3.0 mm. In the bright regions, the intensity of central parts (triangle) is higher than that of the surrounding areas (arrows). (c) A high-magnification image with Masson's trichrome stain; image size is 2.1 × 1.6 mm. The central steatosis part of the acini (indicated by the triangle) corresponds to the brightest regions in the ultrasound image (also indicated by the triangle in (b)). The pericentral areas of the acini corresponding to the less-bright regions in the ultrasound image (arrows in (b)) are indicated by arrows. (d) A high-magnification image with periodic acid-Schiff stain; image size is 2.1 × 1.6 mm. The pericentral areas of the acini show a strong positive reaction to the special stain for glycogen (arrows).

age shown in Fig. 6c, the central brightest regions in the ultrasound images correspond to the steatosis areas (indicated by the triangle); the less-bright areas in the ultrasound images correspond to the gray pericentral parts of the acinus (indicated by the arrows). These pericentral parts had a positive reaction (indicated by the arrows in Fig. 6d) to the periodic acid-Schiff stain which is a special stain for glycogen (Hammad et al. 1982). This showed that 25-MHz ultrasound can also potentially detect the glycogen storage area, where the image intensity is lower than in the steatosis area. With conventional ultrasound, the livers in patients with glycogen storage disease or hepatic glycogenosis are frequently diagnosed as steatosis liver (Chatila and West 1996; Lee et al. 1994). With high-frequency ultrasound, the glycogen storage areas can be further differentiated, making noninvasive studies of glycogen metabolism possible.

In conclusion, the 25-MHz ultrasound images resulted in more accurate steatosis classification. However, future clinical applications will require the limitations of poor penetration depth and small focal zone to be overcome.

Acknowledgments—The authors would like to thank the National Science Council of the Republic of China for financially supporting this research under grant no. NSC 93–2213-E-002–119 and Mr. Chao-Kang Liao for photographic assistance. The reviewers' comments are also greatly appreciated.

REFERENCES

Angulo P. Nonalcoholic fatty liver disease. N Engl J Med 2002;346: 1221–1231.

Brunt EM, Janney CG, Di Bisceglie AM, Neuschwander-Tetri BA, Bacon BR. Nonalcoholic steatohepatitis: a proposal for grading and staging the histological lesions. Am J Gastroenterol 1999;94:2467–2474.

Brunt EM. Nonalcoholic steatohepatitis: definition and pathology. Semin Liver Dis 2001;21:3–16.

Buma T, Spisar M, O'Donnell M. A high-frequency, 2-D array element using thermoelastic expansion in PDMS. IEEE Trans Ultrason Ferroelectr Freq Control 2003;50:1161–1176.

Burges CJC. A tutorial on support vector machines for pattern recognition. Data Mining Knowl Discov 1998;2:955–974.

Chan K, Lee TW, Sample PA, et al. Comparison of machine learning and traditional classifiers in glaucoma diagnosis. IEEE Trans Biomed Eng 2002;49:963–974.

Chatila R, West AB. Hepatomegaly and abnormal liver tests due to glycogenosis in adults with diabetes. Medicine (Baltimore) 1996; 75:327–333.

Cortes C, Vapnik V. Support vector networks. Mach Learn 1995;20: 273–-297.

Dent CL, Scott MJ, Wickline SA, Hall CS. High-frequency ultrasound for quantitative characterization of myocardial edema. Ultrasound Med Biol 2000;26:1375–1384.

Edmonson HA, Peters RL. Liver. In: Kissane JM, ed. Anderson's pathology, 8th edition. St. Louis: Mosby, 1985:1096–1212.

Foster FS, Zhang MY, Zhou YQ, et al. A new ultrasound instrument for *in vivo* microimaging of mice. Ultrasound Med Biol 2002;28:1165–1172.

Fox MD, Pruehsner WR. High frequency ultrasound tissue characterization. IEEE Ultrason Symp 1997:44–45.

Hammad ES, Striffler JS, Cardell RR Jr. Morphological and biochemical observations on hepatic glycogen metabolism in genetically diabetic (db/db) mice. Diabetes Metab 1982;8:147–153.

Haralick RM, Shanmugan K, Dinstein I. Texture features for image classification. IEEE Trans Syst Man Cybern 1973;SMC-3:610–621.

Joseph AE, Saverymuttu SH, al-Sam S, Cook MG, Maxwell JD. Comparison of liver histology with ultrasonography in assessing diffuse parenchymal liver disease. Clin Radiol 1991;43:26–31.

Lee P, Mather S, Owens C, Leonard J, Dicks-Mireaux C. Hepatic ultrasound findings in the glycogen storage diseases. Br J Radiol 1994;67:1062–1066.

Li ML, Chen YF, Guan WJ, Li PC. A digital ultrasonic system for small animal imaging. Ultrason Imaging 2004;26:85–99.

Mojsilovic A, Popovic M, Markovic S, Krstic M. Characterization of visually similar diffuse diseases from B-scan liver images using nonseparable wavelet transform. IEEE Trans Med Imaging 1998; 17:541–549.

Ney H, Essen U, Kneser R. On the estimation of "small" probability by leave-one-out method. IEEE Trans Pattern Anal Machine Intell 1995;17:1202–1212.

Nissen SE, Yock P. Intravascular ultrasound: novel pathophysiological insights and current clinical applications. Circulation 2001;103: 604–616.

Nouby-Mahmoud G, Silverman RH, Coleman DJ. Using high-frequency ultrasound to characterize intraocular foreign bodies. Ophthalmic Surg 1993;24:94–99.

Passmann C, Ermert H. A 100-MHz ultrasound imaging system for dermatologic and ophthalmologic diagnostics. IEEE Trans Ultrason Ferroelectr Freq Control 1996;43:545–552.

Petersen B. Intravascular ultrasound-guided direct intrahepatic portacaval shunt: description of technique and technical refinements. J Vasc Interv Radiol 2003;14:21–32.

Raju BI, Swindells KJ, Gonzalez S, Srinivasan MA. Quantitative ultrasonic methods for characterization of skin lesions *in vivo.* Ultrasound Med Biol 2003;29:825–838.

Teli MR, James OFW, Burt AD, Bennett MK, Day CP. The natural history of nonalcoholic fatty liver: a follow-up study. Hepatology 1995;22:1714–1719.

Wachsberg RH, Angyal EA, Klein KM, Kuo HR, Lambert WC. Echogenicity of hepatic versus portal vein walls revisited with histologic correlation. J Ultrasound Med 1997;16:807–810.

Weiss SM. Small sample error rate estimation for *k*-NN classification. IEEE Trans. Pattern Anal Machine Intell 1991;13:285–289.

Wu C, Chen Y, Hsieh K. Texture features for classification of ultrasonic liver images. IEEE Trans Med Imaging 1992;11:141–152.

Yang PM, Huang GT, Lin JT, et al. Ultrasonography in the diagnosis of benign diffuse parenchymal liver diseases: a prospective study. Taiwan Yi Xue Hui Za Zhi—J Formosan Med Assoc 1988;87:966–977.

Yeh WC, Huang SW, Li PC. Liver fibrosis grade classification with B-mode ultrasound. Ultrasound Med Biol 2003;29:1229–1235.

Yoshihara S, Kubota A, Nishimura T, Hatori M, Saito M. Ultrasonic tissue characterization 30 MHz to 70 MHz on a fatty hen liver. IEEE Eng Med Biol Symp 1998;20:785–788.